Convective instabilities during the solidification of an ideal ternary alloy in a mushy layer

DANIEL M. ANDERSON[1,2]†, GEOFFREY B. McFADDEN[2], SAM R. CORIELL[3] AND BRUCE T. MURRAY[2,4]

[1]Department of Mathematical Sciences, George Mason University, Fairfax, VA 22030, USA

[2]Mathematical and Computational Sciences Division, National Institute of Standards and Technology, Gaithersburg, MD 20899, USA

[3]Metallurgy Division, National Institute of Standards and Technology, Gaithersburg, MD 20899, USA

[4]Department of Mechanical Engineering, State University of New York at Binghamton, Binghamton, NY 13902, USA

We consider a model for the solidification of an ideal ternary alloy in a mushy layer that incorporates the effects of thermal and solutal diffusion, convection and solidification. Our results reveal that although the temperature and solute fields are constrained to the liquidus surface of the phase diagram, the system still admits double-diffusive modes of instability. Additionally, modes of instability exist even in situations in which the thermal and solute fields are each individually stable from a static point of view. We identify these instabilities for a general model in which the base-state solution and its linear stability are computed numerically. We then highlight these instabilities in a much simpler model that admits an analytical solution.

1. Introduction

In the most basic notion of buoyant convection, a light fluid region above a heavy fluid region in a gravitational field represents a stable configuration, while a heavy fluid region above a light fluid region represents a potentially unstable configuration. In the latter case, for a motionless fluid layer to begin to convect, the buoyant forces must be sufficient to overcome viscous and other resistive forces present in the fluid. For a pure fluid whose density decreases with temperature, thermally driven convection could thus commence given an ample supply of heat from below. Similarly, in an isothermal two-component fluid compositionally driven convection can occur when the composition field gives rise to an adverse density gradient, e.g. (heavier) salty fluid above (lighter) fresher fluid.

When two diffusing fields, for example temperature and concentration, are present in the same system the characterization of buoyant convection becomes at once both more complicated and more interesting. In such cases, one must first recognize that the fluid density depends in general on both the temperature and species concentration of the fluid. However, it is also crucial to recognize that the two diffusing quantities can have different diffusivities. These are the key factors controlling the phenomena

† Email address for correspondence: danders1@gmu.edu

of double-diffusive convection (e.g. Turner 1973; Huppert & Turner 1981). In this setting it is possible for a statically stable system (i.e. one whose net density profile is stably stratified) to be linearly unstable to perturbations. Two basic situations can be identified. First, if the slower diffusing component is destabilizing and the faster one is stabilizing, then a direct mode of instability referred to as 'salt fingers' or 'salt fountains' can be present. For a typical case with heat and species diffusion – wherein heat diffuses much more rapidly than species and the fluid density decreases with temperature and increases with salinity – if fresher and cooler fluid is below saltier and warmer fluid, the system is unstable with respect to the slower diffusing composition and salt-finger convection can occur. Here a parcel of fluid displaced upwards equilibrates to its new thermal environment (i.e. warms) relatively quickly but owing to the slow diffusion of species remains relatively fresh (and light) compared with its surroundings, and so the parcel continues to rise. This scenario is known as the 'fingering' regime. On the other hand, if the slower diffusing component is stabilizing and the faster one destabilizing, then the system can admit an over-stable oscillatory instability. Such could be the case with saltier and warmer fluid below fresher and cooler fluid; the faster diffusing thermal field is destabilizing. Here a fluid parcel displaced upwards again equilibrates thermally (i.e. cools) relatively quickly but remains saltier (and heavier) with respect to its new environment. The parcel is forced back down but with a lag in temperature relative to its local environment that effectively adds gravitational mass to the parcel (a similar lag reduces the gravitational mass on an up cycle) and causes it to return to its original position with more inertia than on its previous cycle; the parcel overshoots its original position, and an over-stable oscillation occurs. These oscillations are supported by a stable solute field, and the diffusion of heat allows them to grow. This scenario is known as the 'diffusive' regime.

These ideas have also been extended to describe convection of viscous fluids with three diffusing components. Griffiths (1979) performed a linear stability analysis to assess convection of an isothermal fluid with three diffusing components in a horizontal layer for which the base-state solution consisted of three linear concentration profiles. As in standard double-diffusive convection scenarios when two diffusing components are present, this ternary system admitted direct salt-finger modes as well as over-stable oscillatory modes. A notable result identified by Griffiths (1979) occurs when the fastest and slowest diffusing components contribute the same trends with respect to the density gradient (either both stabilizing or both destabilizing); here salt-finger modes and oscillatory modes can be simultaneously unstable. This can be understood from the perspective of the above-mentioned two-component view of double-diffusive convection by pairing simultaneously the intermediate diffusing component with the faster and the slower diffusing components.

Similar characterizations of double-diffusive convection in porous layers, which are of interest in the present work, can be found in the book by Nield & Bejan (1998). The linear stability problem of double-diffusive convection in a porous layer was originally examined by Nield (1968) and follows closely the ones described above for a viscous fluid. However, one notable difference is that although real modes of instability can occur in the statically stable regions, oscillatory modes, while still present, do not occur in the statically stable regions. Nield's original analysis has been extended to include cases of ternary convection in non-reactive porous layers. Rudraiah & Vortmeyer (1982) repeated the linear stability analysis of Griffiths (1979) for ternary convection in a non-reactive porous layer and reported very similar results. Poulikakos (1985) also presented linear stability results for convection of three diffusing components

in a non-reactive porous layer. These results included the case in which one of the components was a thermal field which, unlike solute, can diffuse equally well through both solid and liquid phases of the porous media.

Buoyant convection often occurs in systems undergoing phase transformation. During the solidification of a binary alloy, for example, both thermal and compositional gradients can be present in the melt, and convection coupled with morphological instabilities of the solid–liquid interface can occur (e.g. see Coriell *et al.* 1980; Hurle, Jakeman & Wheeler 1982; Schaeffer & Coriell 1984; Thi, Billia & Jamgotchian 1989; Lan & Tu 2000). Double-diffusive effects are also known to play important roles in geophysical processes such as magma crystallization (Huppert & Sparks 1984).

It is well known that during solidification of binary alloys, regions known as mushy layers – reactive porous-like regions made up of fine-scale crystals – can form between completely liquid regions and completely solid regions (e.g. see the reviews by Worster 1997, 2000; Davis 2001). Since thermal and solutal gradients can occur in the completely liquid region of such systems the same mechanisms that drive double-diffusive convection in an isolated fluid layer are again present. Further, just as in a non-reactive porous medium, convection driven by thermal and/or solutal gradients within the mushy layer is also possible. However, unlike the case of a non-reactive porous media, the temperature and composition fields in a mushy layer are coupled with the equilibrium phase diagram. In particular, the relatively high surface-area-to-volume ratio of the dendritic crystals in the mushy layer implies that thermodynamic equilibrium is maintained, and for binary alloys this directly couples the temperature T and liquid composition C within the mushy layer through the liquidus constraint $T = T^{\mathscr{L}}(C)$ of the equilibrium phase diagram. Therefore, while the thermal diffusivity is in general much larger than the solutal diffusivity, the temperature and composition within the mushy layer do not behave as independently diffusing quantities owing to the liquidus constraint. This direct coupling therefore eliminates an essential mechanism required for double-diffusive convection. Consequently, while there are a host of interesting, novel and industrially relevant buoyant convective phenomena that occur within binary alloy mushy layers (e.g. Worster 1992*a,b*; Amberg & Homsy 1993; Chen, Lu & Yang 1994; Anderson & Worster 1995, 1996; Schulze & Worster 1998, 1999, 2001; Chung & Chen 2000; Chung & Worster 2002; Guba & Worster 2006*a,b*; Roper, Davis & Voorhees 2007, 2008; Katz & Worster 2008) double-diffusive convection driven from within the mushy layer itself is not one of them. Studies such as those by Nandapurka *et al.* (1989) and Singh & Basu (1995) that specifically refer to double-diffusive, or thermosolutal, convection in binary mushy layer systems still impose the condition of thermodynamic equilibrium within the mushy layer and therefore implicitly refer to double-diffusive convection driven from within completely liquid regions rather than from within a binary mushy layer.

While the understanding of convection in binary mushy layers is by no means complete, there is considerable interest from both industrial and scientific points of view in developing a better understanding of solidification, convection and mushy layer formation in ternary alloy systems. The equilibrium phase diagram for such systems (e.g. Lupis 1993; Smallman & Bishop 1999) can range from relatively simple to highly complex. Systems of interest in metallurgy (e.g. Boettinger *et al.* 1995; Krane & Incropera 1997; Schneider *et al.* 1997; Krane, Incropera & Gaskell 1998; Felicelli, Poirier & Heinrich 1997, 1998) tend to be in the latter category. A fourth, intermetallic phase often further complicates 'ternary' systems. Other recent work has focused on aqueous ternary systems, whose equilibrium phase

diagrams can be characterized relatively easily by a few simple formulas. Laboratory experiments on the aqueous system water–potassium nitrate–sodium nitrate (H_2O–KNO_3–$NaNO_3$) have revealed that in this ternary eutectic system two distinct mushy layers, referred to as the primary and secondary mushy layers, can form between the completely solid and completely liquid layers (Aitta, Huppert & Worster 2001a,b; Thompson *et al.* 2003b). Convection and solidification of another aqueous ternary system H_2O–$CuSO_4$–Na_2SO_4 has also been recently examined (Bloomfield & Huppert 2003).

The primary and secondary mushy layers in these aqueous systems are distinguished by the make-up of the solid material; for example, the solid in the primary layer could be made up of pure ice crystals, while the crystalline matrix of the secondary layer is made up of solid ice and solid potassium nitrate. From the point of view of the equilibrium phase diagram, the primary mushy layer is associated with a liquidus surface, and the secondary mushy layer is associated with a cotectic boundary marking the intersection of two liquidus surfaces. In the primary mushy layer the corresponding thermodynamic equilibrium constraint takes the form $T = T^{\mathscr{L}}(C_1, C_2)$, which states that the temperature and liquid compositions C_1 and C_2 are constrained to lie on the liquidus surface. In the secondary mushy layer two thermodynamic equilibrium constraints of the form $T = T_1^{\mathscr{C}}(C_1)$ and $T = T_2^{\mathscr{C}}(C_2)$ hold for the temperature and compositions along a cotectic boundary. In the secondary mushy layer C_1 and C_2 are directly linked to each other and to T; consequently, these quantities cannot diffuse independently here, and like the binary case, an essential mechanism for double-diffusive convection is absent. In the primary mushy layer, however, there is an additional degree of freedom between the temperature and compositions, as they are linked only through a single constraint $T = T^{\mathscr{L}}(C_1, C_2)$. Does this additional degree of freedom between the temperature and compositions in the primary mush of the ternary system along with thermal and solutal diffusion allow double-diffusive convection to be driven from within a ternary alloy primary mushy layer? More generally, what type of modes are driven from within a primary mushy layer of a ternary alloy? Our objective in the present work is to address these questions.

Previous theoretical studies related to the aqueous ternary alloy systems described above have addressed diffusion-controlled growth of primary and secondary mushy layers without convection (Anderson 2003; Thompson, Huppert & Worster 2003a) and convective effects within primary and secondary mushy layers in the absence of solute diffusion (Anderson & Schulze 2005). While these studies have revealed the rich structure of non-convecting ternary mushy layers as well as both linear and nonlinear convecting states, the existence of double-diffusive convection in general ternary mushy layer systems has not been established. Recently, Flynn (2009) developed a pseudo-spectral numerical scheme to investigate the linear stability of a full three-layer ternary mush problem that extends the work of Anderson & Schulze (2005) to include the effects of solute diffusion. A complete study of this three-layer model is currently underway.

We shall explore in a ternary alloy model the onset of convection within a single primary mushy layer accounting for the effects of both thermal and solutal diffusion. Section 2 outlines the ternary mushy layer model. Section 3 gives the details of the linear stability analysis including the base-state solution, the disturbance equations and numerically computed neutral stability results. Section 4 describes a simple model system deduced from the full ternary model that admits an analytical solution and reveals a new mechanism for instability. Conclusions are given in §5.

2. Ideal ternary mushy layer in a moving frame

We examine a model ternary mushy layer confined between two positions $\tilde{z} = V't'$ and $\tilde{z} = H' + V't'$ that move in time t' at a given constant speed V'. The mushy layer thickness H' is assumed to be a given constant. The fluid density has the form

$$\rho' = \rho^R \left[1 - \alpha(T' - T'_R) - \alpha_1(C'_1 - C'_{1R}) - \alpha_2(C'_2 - C'_{2R})\right], \qquad (2.1)$$

where α and α_j $(j = 1, 2)$ are thermal and solutal expansion coefficients and R indicates a reference state. The governing equations for temperature T', composition C'_1 and C'_2, solid fraction ϕ, pressure p' and Darcy velocity $\boldsymbol{u}'$ in terms of a coordinate frame $z' = \tilde{z} - V't'$ moving with the mushy layer are

$$\bar{c}(\phi) \left[\frac{\partial T'}{\partial t'} - V'\frac{\partial T'}{\partial z'} + \boldsymbol{u}' \cdot \nabla T'\right] = \nabla \cdot \left(\bar{k}(\phi)\nabla T'\right) + L_v \left(\frac{\partial \phi}{\partial t'} - V'\frac{\partial \phi}{\partial z'}\right), \qquad (2.2a)$$

$$(1 - \phi)\left(\frac{\partial C'_j}{\partial t'} - V'\frac{\partial C'_j}{\partial z'}\right) + \boldsymbol{u}' \cdot \nabla C'_j = \nabla \cdot \left(\bar{D}_j(\phi)\nabla C'_j\right) + (1 - k_j)C'_j \left(\frac{\partial \phi}{\partial t'} - V'\frac{\partial \phi}{\partial z'}\right),$$
$$\text{for } j = 1, 2, \qquad (2.2b)$$

$$T' = T'_0 + m'_1 C'_1 + m'_2 C'_2, \qquad (2.2c)$$

$$\boldsymbol{u}' = -\frac{\Pi'(\phi)}{\mu}\left(\nabla p' + \rho' g \hat{\boldsymbol{k}}\right), \qquad (2.2d)$$

$$\nabla \cdot \boldsymbol{u}' = 0, \qquad (2.2e)$$

where $\bar{c}(\phi) = \phi c_s + (1 - \phi)c_l$ is the effective specific heat of the mushy layer with c_s and c_l being the constant specific heat in the solid and liquid phases; $\bar{k}(\phi) = \phi k_s + (1 - \phi)k_l$ is the effective thermal conductivity of the mushy layer with k_s and k_l denoting the constant thermal conductivities in the solid and liquid phases; $\bar{D}_j = (1 - \phi)D_j$ is the solutal diffusivity of the mushy layer with a constant solutal diffusivity D_j in the liquid for species j (diffusion of solute in the solid is neglected); T'_0 is the melting temperature of the pure material; $\Pi'(\phi)$ is the permeability of the mushy layer; μ is the fluid viscosity; g is the gravitational acceleration; and $\hat{\boldsymbol{k}}$ is a unit vector in the z' direction. We assume that the segregation coefficients k_j are constant and that the liquidus slopes m'_j are constant. These equations are the ternary alloy analogues of the ideal binary mushy layer equations described by Worster (1992b, 1997).

In general these equations would be coupled with the dynamics of an adjacent liquid layer and/or other solid or mushy layers. In our simple model, the aim is to isolate the dynamics of the primary mush, and therefore we assume that the composition fields are on a single liquidus surface away from any cotectic or eutectic point. We correspondingly use the boundary conditions

$$T' = T'_{top}, \quad C'_1 = C'_{1top}, \quad \phi = \phi_0, \quad \boldsymbol{u}' \cdot \hat{\boldsymbol{k}} = 0, \quad \text{at } z' = H', \qquad (2.3a)$$

$$T' = T'_{bot}, \quad C'_1 = C'_{1bot}, \quad \boldsymbol{u}' \cdot \hat{\boldsymbol{k}} = 0, \quad \text{at } z' = 0, \qquad (2.3b)$$

where T'_{top}, T'_{bot}, C'_{1top}, C'_{1bot} and ϕ_0 are given constants. Note that since T', C'_1 and C'_2 are coupled by the liquidus constraint (2.2c) we do not impose independent values for composition C'_2. This reduced model will allow convective modes of instability driven from within the primary mushy layer to be examined without the added complication of other convecting layers. This simplifies the mathematical development and, more importantly, allows for a clearer physical interpretation of the instabilities that arise.

2.1. *Non-dimensionalization*

Here we introduce dimensionless forms of the above-given equations. Lengths are scaled with the layer thickness H', time with H'^2/κ, where $\kappa = k_l/c_l$ is the thermal diffusivity, and velocity with κ/H'. We introduce the dimensionless temperature and composition variables

$$T = \frac{T' - T'_{bot}}{\Delta T}, \quad C_j = \frac{C'_j}{\Delta C_j}, \tag{2.4}$$

where $\Delta T = T'_{top} - T'_{bot}$ and $\Delta C_j = C'_{j\,top} - C'_{j\,bot}$ for $j = 1, 2$. For a dimensionless pressure variable we introduce

$$p = \frac{\Pi_0}{\kappa\mu}\left[p' + \rho^R g z'\right], \tag{2.5}$$

where Π_0 is a reference permeability.

The dimensionless governing equations become

$$c(\phi)\left(\frac{\partial T}{\partial t} - V\frac{\partial T}{\partial z} + \boldsymbol{u}\cdot\nabla T\right) = \nabla\cdot(k(\phi)\nabla T) + S\left(\frac{\partial\phi}{\partial t} - V\frac{\partial\phi}{\partial z}\right), \tag{2.6a}$$

$$(1-\phi)\left(\frac{\partial C_j}{\partial t} - V\frac{\partial C_j}{\partial z}\right) + \boldsymbol{u}\cdot\nabla C_j = \frac{1}{Le_j}\nabla\cdot\left[(1-\phi)\nabla C_j\right] + (1-k_j)C_j$$

$$\times\left(\frac{\partial\phi}{\partial t} - V\frac{\partial\phi}{\partial z}\right), \quad \text{for } j = 1, 2 \tag{2.6b}$$

$$T = T_0 + m_1 C_1 + m_2 C_2, \tag{2.6c}$$

$$\boldsymbol{u} = -\Pi(\phi)\left(\nabla p + \Delta\rho\hat{\boldsymbol{k}}\right), \tag{2.6d}$$

$$\nabla\cdot\boldsymbol{u} = 0, \tag{2.6e}$$

where $c(\phi) = (c_s/c_l)\phi + 1 - \phi$, $k(\phi) = (k_s/k_l)\phi + 1 - \phi$, $\Pi(\phi) = \Pi'(\phi)/\Pi_0$ and $\Delta\rho$ represents a density change related to temperature and composition by

$$\Delta\rho = -Ra(T - T^R) - Ra_1\left(C_1 - C_1^R\right) - Ra_2\left(C_2 - C_2^R\right). \tag{2.7}$$

In the current work we take $\Pi(\phi) = (1-\phi)^3$ unless noted otherwise. The dimensionless parameters that appear are

$$V = \frac{V'H'}{\kappa}, \quad S = \frac{L_v}{c_l\Delta T}, \quad Le_j = \frac{\kappa}{D_j}, \quad T_0 = \frac{T'_0 - T'_{bot}}{\Delta T}, \quad T^R = \frac{T'_R - T'_{bot}}{\Delta T}, \tag{2.8a}$$

$$Ra = \frac{\alpha\Delta T g\Pi_0 H'}{\kappa\nu}, \quad Ra_j = \frac{\alpha_j\Delta C_j g\Pi_0 H'}{\kappa\nu}, \quad m_j = \frac{m'_j\Delta C_j}{\Delta T}, \quad C_j^R = \frac{C'_{j\,R}}{\Delta C_j}, \tag{2.8b}$$

for $j = 1, 2$, where $\nu = \mu/\rho^R$. Note that from the liquidus constraint $\Delta T = m'_1\Delta C_1 + m'_2\Delta C_2$, or in dimensionless form $1 = m_1 + m_2$. The boundary conditions are

$$T = 1, \quad C_1 = C_1^{top} \equiv C_1^{bot} + 1, \quad \phi = \phi_0, \quad \boldsymbol{u}\cdot\hat{\boldsymbol{k}} = 0, \quad \text{at } z = 1, \tag{2.9a}$$

$$T = 0, \quad C_1 = C_1^{bot}, \quad \boldsymbol{u}\cdot\hat{\boldsymbol{k}} = 0, \quad \text{at } z = 0, \tag{2.9b}$$

where $C_1^{bot} = C'_{1bot}/\Delta C_1$. In place of the boundary conditions on T we could equivalently impose $C_2(z=0) = C_2^{bot}$, where $C_2^{bot} = -(T_0 + m_1 C_1^{bot})/m_2$ and $C_2(z=1) = C_2^{top} \equiv C_2^{bot} + 1$.

The density in (2.7) depends on T, C_1 and C_2, but these quantities are not all independent owing to the liquidus contraint (2.6c). If we define a density gradient

$$G_\rho = \nabla(\Delta\rho) = -Ra\nabla T - Ra_1\nabla C_1 - Ra_2\nabla C_2 \tag{2.10}$$

and note that by (2.6c) we can eliminate C_2, then

$$G_\rho = -Ra_T\nabla T - Ra_C\nabla C_1. \tag{2.11}$$

Therefore we can quantify buoyant effects through the two effective Rayleigh numbers

$$Ra_T \equiv Ra + \frac{1}{m_2}Ra_2, \quad Ra_C \equiv Ra_1 - \frac{m_1}{m_2}Ra_2. \tag{2.12}$$

Note that $Ra_T + Ra_C = Ra + Ra_1 + Ra_2$.

3. Linear stability analysis

3.1. *Steady base state solution*

Steady, one-dimensional non-convecting solutions to (2.6) satisfy

$$-c(\bar\phi)V\frac{\mathrm{d}\bar T}{\mathrm{d}z} = \frac{\mathrm{d}}{\mathrm{d}z}\left(k(\bar\phi)\frac{\mathrm{d}\bar T}{\mathrm{d}z}\right) - VS\frac{\mathrm{d}\bar\phi}{\mathrm{d}z}, \tag{3.1a}$$

$$-V(1-\bar\phi)\frac{\mathrm{d}\bar C_j}{\mathrm{d}z} = \frac{1}{Le_j}\frac{\mathrm{d}}{\mathrm{d}z}\left[(1-\bar\phi)\frac{\mathrm{d}\bar C_j}{\mathrm{d}z}\right] - V(1-k_j)\bar C_j\frac{\mathrm{d}\bar\phi}{\mathrm{d}z}, \quad \text{for } j=1,2, \tag{3.1b}$$

$$\bar T = T_0 + m_1\bar C_1 + m_2\bar C_2, \tag{3.1c}$$

subject to boundary conditions $\bar T = 1$, $\bar C_1 = C_1{}^{bot} + 1$, $\bar\phi = \phi_0$ at $z=1$ and $\bar T = 0$, $\bar C_1 = C_1{}^{bot}$ at $z=0$. Again note that in place of the boundary conditions on $\bar T$ we could equivalently impose $\bar C_2(z=0) = C_2{}^{bot}$, where $C_2{}^{bot} = -(T_0 + m_1 C_1{}^{bot})/m_2$ and $\bar C_2(z=1) = C_2{}^{bot} + 1$. The equation for $\bar p$ will not be needed in the analysis.

3.1.1. *Base state solution*

We solve the equations for the base-state solution numerically by using a shooting method. In particular, we rewrite the base-state equations as a system of first-order differential equations for quantities $\bar\phi$, $\bar C_1$, $\bar C_2$, Q_1 and Q_2, where

$$Q_j \equiv (1-\bar\phi)\frac{\mathrm{d}\bar C_j}{\mathrm{d}z}, \quad \text{for } j=1,2. \tag{3.2}$$

These equations are

$$m_1\frac{\mathrm{d}Q_1}{\mathrm{d}z} + m_2\frac{\mathrm{d}Q_2}{\mathrm{d}z} = -\frac{c(\bar\phi)}{k(\bar\phi)}V(m_1 Q_1 + m_2 Q_2) + f(Q_1, Q_2, \bar\phi)\frac{\mathrm{d}\bar\phi}{\mathrm{d}z}, \tag{3.3a}$$

$$\frac{1}{Le_1}\frac{\mathrm{d}Q_1}{\mathrm{d}z} = -VQ_1 + V(1-k_1)\bar C_1\frac{\mathrm{d}\bar\phi}{\mathrm{d}z}, \tag{3.3b}$$

$$\frac{1}{Le_2}\frac{\mathrm{d}Q_2}{\mathrm{d}z} = -VQ_2 + V(1-k_2)\bar C_2\frac{\mathrm{d}\bar\phi}{\mathrm{d}z}, \tag{3.3c}$$

$$\frac{\mathrm{d}\bar C_1}{\mathrm{d}z} = \frac{Q_1}{1-\bar\phi}, \tag{3.3d}$$

$$\frac{\mathrm{d}\bar C_2}{\mathrm{d}z} = \frac{Q_2}{1-\bar\phi}, \tag{3.3e}$$
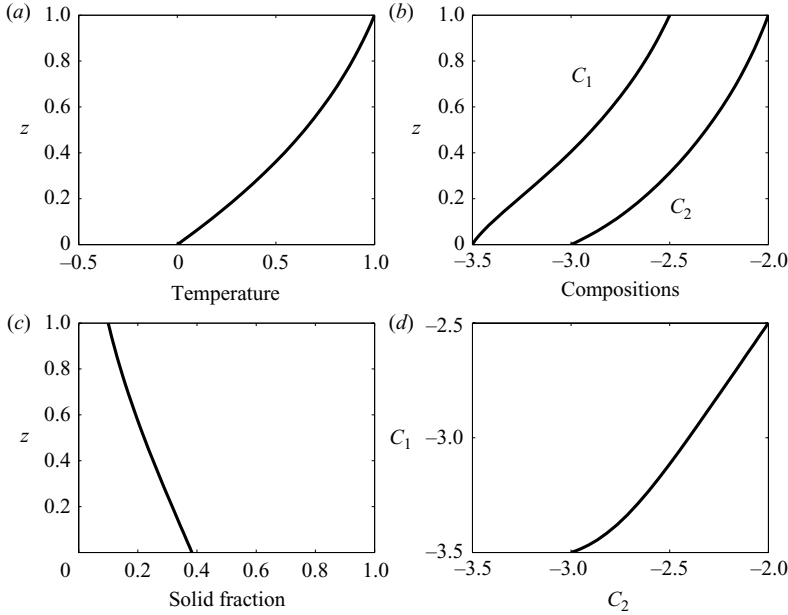
FIGURE 1. The figure shows a typical base-state solution for the ternary alloy model. The parameter values used here are $m_1 = m_2 = 0.5$, $k_1 = k_2 = 0.1$, $Le_1 = Le_2 = 100$, $S = 37$, $k_s/k_l = 1$, $c_s/c_l = 1$, $V = 0.1$, $\phi_0 = 0.1$, $C_1^{bot} = -3.5$ and $C_2^{bot} = -3$.

where

$$f(Q_1, Q_2, \bar{\phi}) = -\frac{m_1 Q_1 + m_2 Q_2}{1 - \bar{\phi}} + \frac{V S(1 - \bar{\phi})}{k(\bar{\phi})} - \frac{1}{k(\bar{\phi})}\frac{\mathrm{d}k}{\mathrm{d}\bar{\phi}}(m_1 Q_1 + m_2 Q_2). \quad (3.4)$$

Using (3.3b) and (3.3c) we find that (3.3a) can be written in the form

$$\frac{\mathrm{d}\bar{\phi}}{\mathrm{d}z} = -\frac{V\left[m_1 Le_1 Q_1 + m_2 Le_2 Q_2 - (c(\bar{\phi})/k(\bar{\phi}))(m_1 Q_1 + m_2 Q_2)\right]}{f - V\left[m_1 Le_1(1 - k_1)\bar{C}_1 + m_2 Le_2(1 - k_2)\bar{C}_2\right]}. \quad (3.5)$$

The shooting procedure involves integrating (3.3b)–(3.3e) and (3.5) subject to the conditions $\bar{C}_1 = C_1^{top}$, $\bar{C}_2 = C_2^{top}$, $\bar{\phi} = \phi_0$ and $Q_j = Q_j^{top}$ for $j = 1, 2$ at $z = 1$. The conditions on Q_j are used as shooting parameters iteratively chosen to satisfy the conditions $\bar{C}_1 = C_1^{bot}$ and $\bar{C}_2 = C_2^{bot}$ at $z = 0$. These calculations are done using Matlab with `ode23s` for the integration and `fsolve` to solve the nonlinear system for the two unknowns Q_j^{top}. For use in the pseudo-spectral linear stability calculations to follow, the base-state solution is output at N_P Chebyshev points. A typical base-state solution, which reveals nonlinear temperature, composition and solid fraction profiles, is shown in figure 1. Figure 1(d) shows a projection of the solution on to the C_1–C_2 plane (other examples are shown in figure 7). While the composition profiles shown here are monotonic throughout the layer, we show in more detail below that for other sets of parameters the composition profiles can be non-monotonic.

3.2. *Linearized disturbance equations*

In order to study the linear stability of the base-state solutions given above we introduce perturbations of the form

$$T = \bar{T}(z) + \left[\hat{T}(z)\mathrm{e}^{\sigma t + iax} + \text{c.c.}\right], \quad (3.6a)$$

$$C_j = \bar{C}_j(z) + \left[\hat{C}_j(z)\mathrm{e}^{\sigma t + iax} + \text{c.c.}\right], \tag{3.6b}$$

$$\boldsymbol{u} = 0 + \left[(\hat{u}(z), 0, \hat{w}(z))\mathrm{e}^{\sigma t + iax} + \text{c.c.}\right], \tag{3.6c}$$

$$\phi = \bar{\phi}(z) + \left[\hat{\phi}(z)\mathrm{e}^{\sigma t + iax} + \text{c.c.}\right], \tag{3.6d}$$

$$p = \bar{p}(z) + \left[\hat{p}(z)\mathrm{e}^{\sigma t + iax} + \text{c.c.}\right], \tag{3.6e}$$

where σ is a complex growth rate and a is a horizontal wavenumber.

After eliminating the variables $\hat{u}$, $\hat{p}$ and $\hat{C}_2$ the linear disturbance equations are

$$\left[k(\bar{\phi})\right] D^2\hat{T} + \left[k'(\bar{\phi})D\bar{\phi} + c(\bar{\phi})V\right] D\hat{T} - \left[a^2 k(\bar{\phi})\right]\hat{T} - \left[c(\bar{\phi})D\bar{T}\right]\hat{w} + \left[k'(\bar{\phi})D\bar{T}\right.$$
$$\left. -SV\right]D\hat{\phi} + \left[k'(\bar{\phi})D^2\bar{T} + k''(\bar{\phi})D\bar{\phi}D\bar{T} + Vc'(\bar{\phi})D\bar{T}\right]\hat{\phi} = \sigma\{c(\bar{\phi})\hat{T} - S\hat{\phi}\}, \tag{3.7a}$$

$$\left[\frac{1-\bar{\phi}}{Le_1}\right] D^2\hat{C}_1 + \left[V(1-\bar{\phi}) - \frac{D\bar{\phi}}{Le_1}\right] D\hat{C}_1 - \left[\frac{a^2(1-\bar{\phi})}{Le_1} + V(1-k_1)D\bar{\phi}\right]\hat{C}_1$$
$$- \left[D\bar{C}_1\right]\hat{w} - \left[\frac{D\bar{C}_1}{Le_1} + V(1-k_1)\bar{C}_1\right]D\hat{\phi} - \left[\frac{D^2\bar{C}_1}{Le_1} + VD\bar{C}_1\right]\hat{\phi}$$
$$= \sigma\{(1-\bar{\phi})\hat{C}_1 - (1-k_1)\bar{C}_1\hat{\phi}\}, \tag{3.7b}$$

$$\frac{1}{m_2}\left[\frac{1-\bar{\phi}}{Le_2}\right] D^2\hat{T} + \frac{1}{m_2}\left[V(1-\bar{\phi}) - \frac{D\bar{\phi}}{Le_2}\right] D\hat{T} - \frac{1}{m_2}\left[\frac{a^2(1-\bar{\phi})}{Le_2} + V(1-k_2)D\bar{\phi}\right]\hat{T}$$
$$- \frac{m_1}{m_2}\left[\frac{1-\bar{\phi}}{Le_2}\right] D^2\hat{C}_1 - \frac{m_1}{m_2}\left[V(1-\bar{\phi}) - \frac{D\bar{\phi}}{Le_2}\right] D\hat{C}_1 + \frac{m_1}{m_2}\left[\frac{a^2(1-\bar{\phi})}{Le_2}\right.$$
$$\left. + V(1-k_2)D\bar{\phi}\right]\hat{C}_1 - \left[D\bar{C}_2\right]\hat{w} - \left[\frac{D\bar{C}_2}{Le_2} + V(1-k_2)\bar{C}_2\right]D\hat{\phi}$$
$$- \left[\frac{D^2\bar{C}_2}{Le_2} + VD\bar{C}_2\right]\hat{\phi} = \sigma\{\frac{1-\bar{\phi}}{m_2}(\hat{T} - m_1\hat{C}_1) - (1-k_2)\bar{C}_2\hat{\phi}\}, \tag{3.7c}$$

$$D^2\hat{w} - \left(\frac{1}{\Pi(\bar{\phi})}\frac{\mathrm{d}\Pi}{\mathrm{d}\bar{\phi}}D\bar{\phi}\right) D\hat{w} - a^2\hat{w} + a^2\Pi(\bar{\phi})\left[Ra_T\hat{T} + Ra_C\hat{C}_1\right] = 0, \tag{3.7d}$$

where $D = d/dz$. These disturbance equations are subject to the boundary conditions

$$\hat{T} = \hat{C}_1 = \hat{w} = \hat{\phi} = 0, \qquad \text{at } z = 1, \tag{3.8a}$$
$$\hat{T} = \hat{C}_1 = \hat{w} = 0, \qquad \text{at } z = 0. \tag{3.8b}$$

The governing equations can be interpreted as (i) an equation for temperature (3.7a), (ii) an equation for composition $\hat{C}_1$ (3.7b), (iii) an equation for solid fraction (3.7c) and (iv) an equation for the vertical flow (3.7d). Note that the buoyancy terms in (3.7d) involve two independent Rayleigh numbers: an effective thermal Rayleigh number multiplying $\hat{T}$ and an effective solutal Rayleigh number multiplying $\hat{C}_1$, all coupled with the solidification via the solid fraction perturbation $\hat{\phi}$.

3.3. *Ternary alloy stability results*

The above-given linear disturbance equations are solved with a pseudo-spectral Chebyshev method (Canuto *et al.* 1988; Trefethen 2000) in which we discretize the vertical direction through the layer with N_P Chebyshev points. This leads to a generalized eigenvalue problem that determines the growth rate σ and eigenfunctions

in terms of the perturbation wavenumber and the system parameters. Such an approach was also used in the linear stability calculations of Anderson & Schulze (2005). We have validated this approach by implementing another numerical scheme based on a shooting-type method of Keller (1976) in which the resulting boundary-value problems are integrated using the SUPORT code (Scott & Watts 1977). Our numerical approach has also been validated by comparison with the analytical formulas presented later in § 4.

There is a large body of work on binary mushy layer models, and it is instructive to understand under what conditions the present ternary system (2.6) reduces to an effective binary one. Specifically, we shall outline briefly here conditions under which the density gradient, using the liquidus constraint, can be expressed in terms of the gradient of a single independent variable (e.g. temperature). In particular, we identify two scenarios. (i) Our ternary alloy system reduces to an effective binary one when $Le_1 = Le_2$, $k_1 = k_2$ and $m_2' \alpha_1 = m_1' \alpha_2$. The latter assumption can also be expressed as the condition $m_2 Ra_1 = m_1 Ra_2$ or from (2.12) that $Ra_C = 0$. This leads to a system of equations equivalent to those described in Worster (1992b) in which the density gradient can be expressed explicitly in terms of the temperature gradient, $G_\rho = -Ra_T \nabla T$. (ii) A second scenario in which a binary alloy model can be recovered involves the assumptions $Le_1 = Le_2$, $k_1 = k_2$ as well as the condition that the composition boundary values are equal $C_1^{bot} = C_2^{bot} \equiv C^{bot}$. In this case, the density gradient can again be expressed exclusively in terms of a thermal gradient, $G_\rho = -(Ra_T + Ra_C)\nabla T$, and the system again is equivalent to the binary alloy model of Worster (1992b).

Two key observations regarding binary mushy layer instabilities most relevant for the understanding of the ternary alloy instabilities are (i) no binary alloy instabilities occur in a statically stable region and (ii) both real and oscillatory modes are present, and either type can be the most dangerous. Such oscillatory modes have been observed and documented in a study of convection in a single-layer binary mushy layer by Anderson & Worster (1996). These oscillatory modes are not double diffusive in nature; the temperature and composition cannot diffuse independently in the binary system (or effective binary system derived from the ternary model under assumptions (i) or (ii)) owing to the direct coupling through the binary liquidus constraint.

With the above-mentioned points in mind, we now examine the full ternary model. Figure 2 shows C_1 and C_2 profiles for five numerically computed base-state solutions with different boundary values C_1^{bot} and C_2^{bot}. The dashed line shows cases in which $C_1 = C_2$ throughout the layer corresponding to the effective binary case (ii). Regions 2 and 4 between the solid and dashed lines show where the C_1 and C_2 profiles are both monotonically increasing functions of z throughout the layer. Region 1 shows where the C_2 profile varies non-monotonically in space and exhibits a boundary layer near $z = 0$. Similarly, region 5 shows where the C_1 profile varies non-monotonically. The thermal profile is in all cases monotonically increasing. Owing to the symmetry with respect to compositions C_1 and C_2 we shall focus our attention primarily on base-state solutions 4 and 5. This figure provides a means of anticipating modes of instability associated with individual solute components by identifying where the solute contributes towards a positive density gradient (e.g. where $-Ra_j d\bar{C}_j/dz$ is positive in (2.10)). If one examines base-state solution 5 one would expect, for example, two standard modes of buoyant instabilities with respect to the C_1 profile: one with $Ra_1 < 0$ in which the upper portion of the layer, where $d\bar{C}_1/dz > 0$, is gravitationally unstable and one with $Ra_1 > 0$ in which the lower boundary layer, where $d\bar{C}_1/dz < 0$,
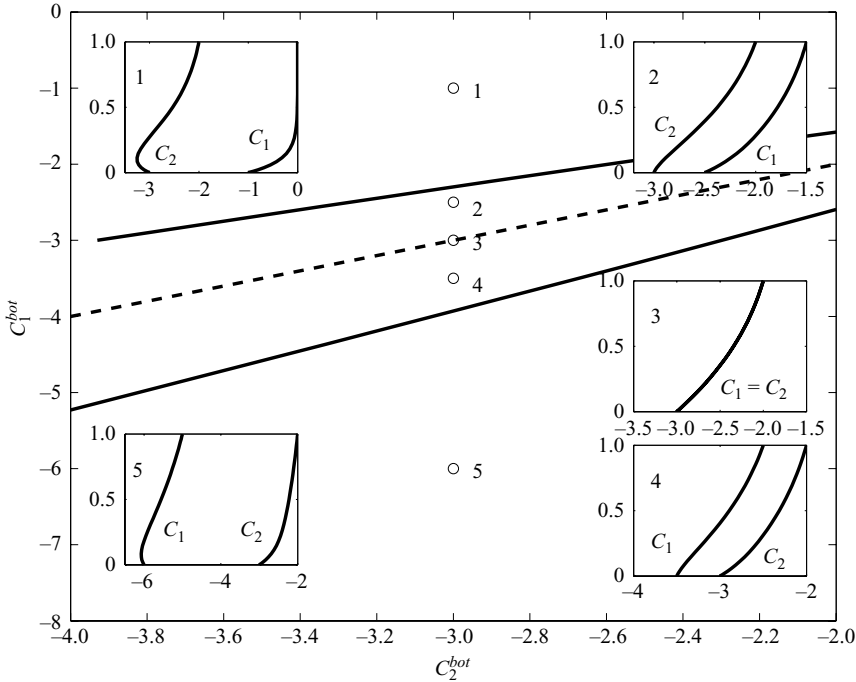
FIGURE 2. This plot shows five characteristic base-state composition profiles (z versus composition) and the regions in the C_1^{bot}-versus-C_2^{bot} plane in which they occur. The parameter values used are $m_1 = m_2 = 0.5$, $Le_1 = Le_2 = 100$, $k_1 = k_2 = 0.1$, $S = 37$, $k_s/k_l = 1$, $c_s/c_l = 1$ $V = 0.1$, $\phi_0 = 0.1$ and $N_P = 32$ with values C_1^{bot} and C_2^{bot} as shown.

is gravitationally unstable. Similarly, for base-state solution 4 one might anticipate that only $Ra_1 < 0$ would give rise to a gravitationally unstable density profile with respect to C_1. Surprisingly, however, we find additional modes of instability associated with different mechanisms.

Examples of neutral stability curves Ra_T versus a with fixed Ra_C are shown in figure 3 for base-state solution 4. The lower curve with $Ra_C = -21.2$ shows the structure of the neutral stability curve near the transition between a real mode (indicated by ○) and an oscillatory mode (indicated by ×). Indicated are the regions in which one unstable real mode is present (denoted by A), two unstable oscillatory modes are present (denoted by B) and two unstable real modes are present (denoted by C, located in a very narrow region between a boundary marked with circles that extends the real neutral curve and another with triangles). The same underlying structure occurs for the upper curve with $Ra_C = -21.3$ in figure 3, but only the most dangerous portions are shown for clarity. These two values of Ra_C were chosen to demonstrate the transition in the most dangerous mode from real to oscillatory that occurs along with a discontinuous jump in the critical wavenumber. This basic modal structure was also identified in the binary alloy model of Anderson & Worster (1996). While the oscillatory mode shown here appears to be an extension of this binary oscillatory mode into the ternary regime we also note that in a simplified ternary model presented in the next section, a ternary oscillatory mode is present even when the required elements (such as non-zero pulling speed V and non-zero latent heat) of the binary oscillatory mode of Anderson & Worster (1996) are absent.
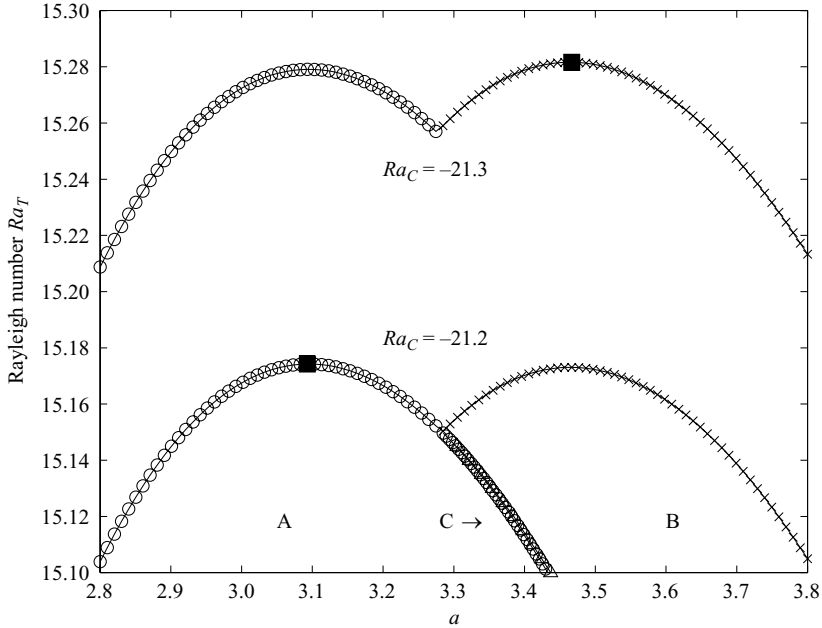
FIGURE 3. This plot shows neutral stability curves for two different values of Ra_C near the transition between real ($\bigcirc$) and oscillatory ($\times$) modes. The lower curves also indicate further structure of these modes and the regions with one unstable real mode (denoted by A), two unstable oscillatory modes (denoted by B) and two unstable real modes (denoted by C). The parameter values used here (corresponding to solution 4 shown in figure 2) are $m_1 = m_2 = 0.5$, $Le_1 = Le_2 = 100$, $k_1 = k_2 = 0.1$, $S = 37$, $k_s/k_l = 1$, $c_s/c_l = 1$, $V = 0.1$, $\phi_0 = 0.1$, $C_1^{bot} = -3.5$, $C_2^{bot} = -3$ and $N_P = 32$.

Neutral stability boundaries Ra_C versus a (fixed Ra_T) shown in figure 4 reveal a more striking view of the instabilities associated with base-state solution 4. Two distinct neutral stability branches occur for $Ra_T = 0$ that separate linearly unstable regions (above the upper curve and below the lower curve) from a linearly stable region in between. Note that along the lower $Ra_T = 0$ curve as well as on other curves in figure 4 we have again shown only the most dangerous portion of the neutral stability curve (as in the upper curve of figure 3). This result indicates that an instability is possible for either sufficiently positive or sufficiently negative values of Ra_C. Interestingly, one possible combination of Ra, Ra_1 and Ra_2 corresponding to $Ra_T = 0$ is $Ra = Ra_2 = 0$ and Ra_1 either positive or negative depending on the solution branch. For $Ra_1 > 0$ this identifies a base-state solution that is statically stable ($G_\rho = -Ra_1 d\bar{C}_1/dz < 0$) but is apparently dynamically unstable. While modes with $Ra_1 > 0$ and modes with $Ra_1 < 0$, driven by a standard buoyant fluid mechanism, would be expected to occur when a non-monotonic composition profile such as that in base-state solution 5 is present, the presence of a mode with $Ra_1 > 0$ for base-state solution 4 is not explained by this mechanism. A new mechanism, which will be described in the next section, is needed. Similar neutral curves are shown for $Ra_C = -15$ and -30 where again two distinct unstable regions are separated by an intermediate stable region. Between $Ra_T = -30$ and $Ra_T = -40$ the upper and lower neutral branches meet at a saddle point, and for $Ra_T = -40$ two regions of linear stability are separated by a region of linear instability; there is a window of wavenumbers between which the system is linearly unstable for any value of Ra_C.
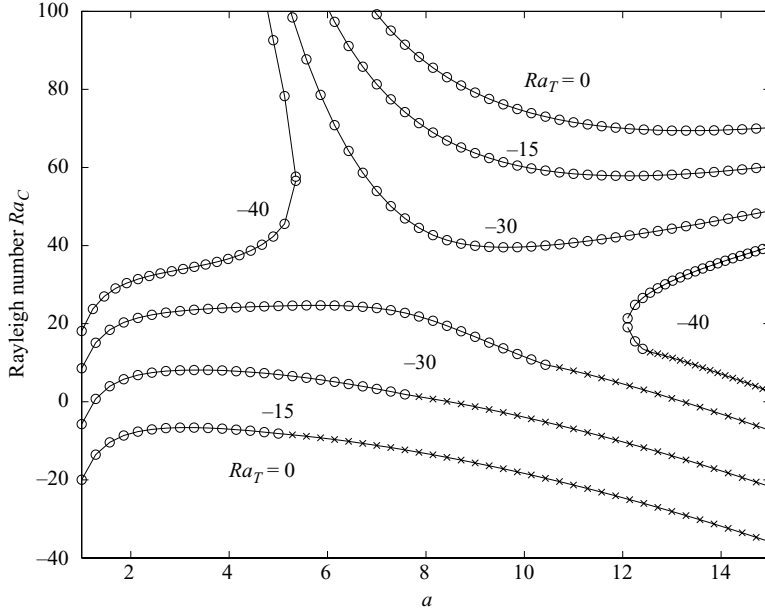
FIGURE 4. This figure shows the most dangerous portions of four sets of neutral stability curves Ra_C versus a for different fixed values of Ra_T as shown. For the case $Ra_T = 0$ the two boundaries separate linearly unstable regions above the upper curve and below the lower curve from a linearly stable region in between the two curves. For $Ra_T = -15$ and $Ra_T = -30$ the stable and unstable regions are similarly positioned. For the case $Ra_T = -40$ an unstable region now separates two stable regions on the left and the right. The parameter values used here (corresponding to solution 4 shown in figure 2) are $m_1 = m_2 = 0.5$, $Le_1 = Le_2 = 100$, $k_1 = k_2 = 0.1$, $S = 37$, $k_s/k_l = 1$, $c_s/c_l = 1$, $V = 0.1$, $\phi_0 = 0.1$, $C_1^{bot} = -3.5$, $C_2^{bot} = -3$ and $N_P = 32$.

Figures 5 and 6 show a broader view of the stability boundaries for base-state solutions 4 and 5 in which we track the critical point of the neutral stability curves (e.g. the points marked by the solid boxes in figure 3) in the Ra_C-versus-Ra_T space. In figure 5, for base-state solution 4, the stability boundary separating stable regions (on the right) from unstable regions (on the left) comprise both real ($\circ$) and complex ($\times$) portions. The shaded regions (either yellow or cyan) indicate where the base-state solution is statically stable. The cyan-coloured region further indicates where it is possible for Ra, Ra_1 and Ra_2 to be all simultaneously positive. The dashed lines show the directions in which Ra varies with Ra_1 and Ra_2 fixed (horizontal line), Ra_1 varies with Ra and Ra_2 fixed (vertical line) and Ra_2 varies with Ra and Ra_1 fixed (diagonal dash-dotted line). Of particular note is that the real portion of the stability boundary extends both into the statically stable region, as could be anticipated for a double-diffusive instability, and into the region in which Ra, Ra_1 and Ra_2 all positive is possible. The latter fact suggests an instability mechanism that can drive convection even when the thermal and solute fields are individually stably stratified. The upper inset shows the streamfunction perturbation at the point with $Ra_C = 60$ in the main plot. This is a real mode with relatively small-scale convection cells localized near the bottom of the mushy layer and has $\omega = 0$, $a = 12.34$ and $Ra_T = -12.48$. The lower inset shows a snapshot in time of the streamfunction perturbation for an oscillatory mode at the point with $Ra_C = -40$ in the main plot. This oscillatory mode has $\omega = 0.2711$, $a = 3.41$ and $Ra_T = 35.57$.
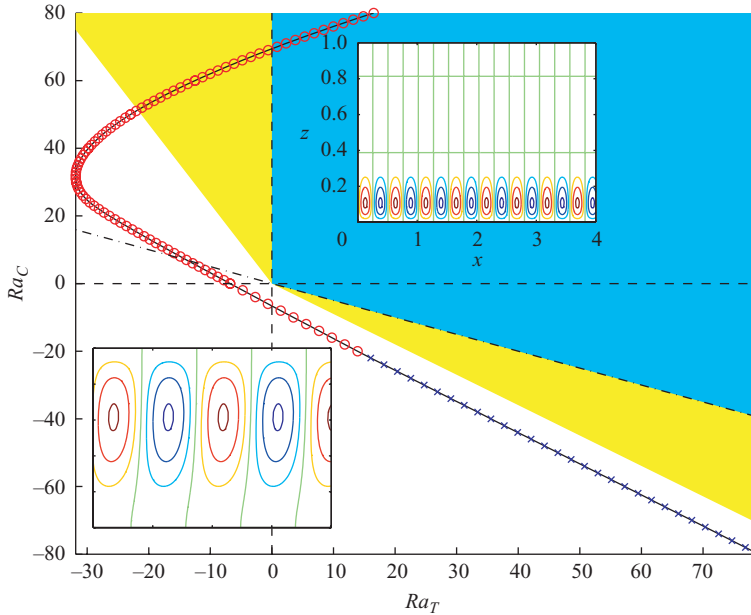
FIGURE 5. This figure shows the critical set of Ra_T and Ra_C values at neutral stability ($\circ$ for real portions and $\times$ for oscillatory portions) for base-state solution 4 in figure 2. The shaded regions show where the base-state solution is statically stable. The cyan-coloured region shows where it is possible for Ra, Ra_1 and Ra_2 to be all simultaneously positive. The dashed lines show the directions in which Ra varies with Ra_1 and Ra_2 fixed (horizontal line), Ra_1 varies with Ra and Ra_2 fixed (vertical line) and Ra_2 varies with Ra and Ra_1 fixed (diagonal dash-dotted line). The parameter values used here are $m_1 = m_2 = 0.5$, $Le_1 = Le_2 = 100$, $k_1 = k_2 = 0.1$, $S = 37$, $k_s/k_l = 1$, $c_s/c_l = 1$, $V = 0.1$, $\phi_0 = 0.1$, $C_1^{bot} = -3.5$, $C_2^{bot} = -3$ and $N_P = 32$.

Figure 6 shows the stability boundary for base-state solution 5. In contrast with base state 4, there is no (cyan) region in which the density is stably stratified with respect to all fields; that is to say while the region in the Ra_C-versus-Ra_T plane where Ra, Ra_1 and Ra_2 are all positive is the same as before, for this particular base state $d\bar{C}_1/dz$ changes signs in the layer, and hence any non-zero value of Ra_1 would imply the existence of a potentially unstable configuration with respect to C_1 based on a standard buoyancy argument. Along the vertical dashed line, which could be interpreted as modes with $Ra = Ra_2 = 0$ and Ra_1 non-zero, two neutral modes of instability occur outside the region of static stability and correspond to the destabilization of either the boundary layer region near the bottom of the layer or the main portion of the layer. The upper inset shows the streamfunction perturbation at the point with $Ra_C = 15$ in the main plot. This is a real mode with relatively small-scale convection cells localized near the bottom of the mushy layer and has $\omega = 0$, $a = 13.42$ and $Ra_T = 65.78$. The lower inset shows the streamfunction perturbation at the point with $Ra_C = -40$ in the main plot. This is an oscillatory mode that has $\omega = 0.65$, $a = 3.37$ and $Ra_T = 44.12$.

The set of calculations shown here indicates the presence of modes of instability that cannot be described by known mechanisms. In the next section we present a simplified model, derived from our original one, that admits analytical solutions. More importantly, these solutions reveal a new mechanism for instability that occurs in ternary mushy layers.
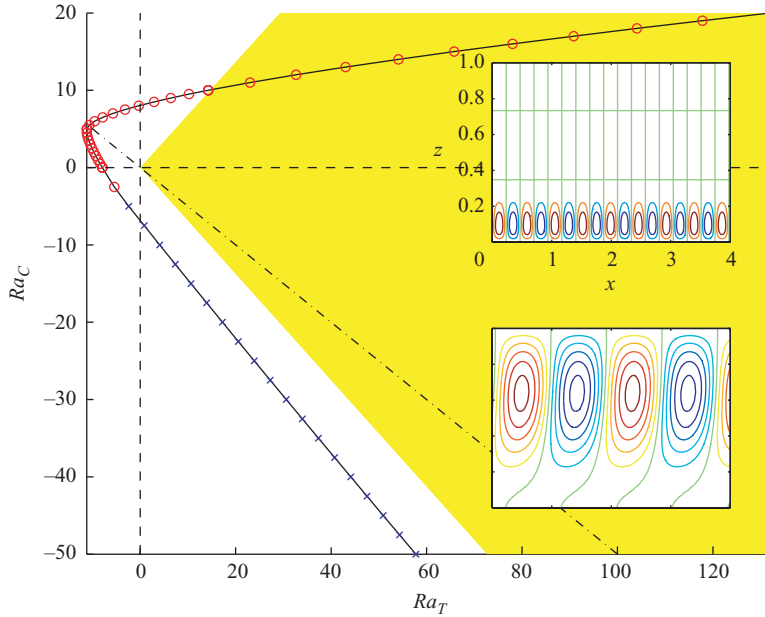
FIGURE 6. This figure shows the critical set of Ra_T and Ra_C values at neutral stability (marked by $\circ$ for real portions and $\times$ for oscillatory portions) for base-state solution 5 in figure 2. The parameter values used here are $m_1 = m_2 = 0.5$, $Le_1 = Le_2 = 100$, $k_1 = k_2 = 0.1$, $S = 37$, $k_s/k_l = 1$, $c_s/c_l = 1$, $V = 0.1$, $\phi_0 = 0.1$, $C_1^{bot} = -6$, $C_2^{bot} = -3$ and $N_P = 32$.

4. A new mechanism for instability

The disturbance equations (3.7a)–(3.7d), while simplified considerably from a full ternary alloy model in which a liquid layer and secondary mushy layer are also present (e.g. Anderson & Schulze 2005; Flynn 2009), are still too difficult to solve analytically. In this section we identify a special case in which an analytical solution is possible. More importantly, the scenarios examined here allow for a clear identification of a new mechanism for instability that is much better disguised in results of the full model.

Consider (3.7a)–(3.7d) under the assumptions that $c(\bar\phi) = k(\bar\phi) = \Pi(\bar\phi) = 1$ and $V = S = 1 - k_j = 0$. The corresponding base-state solution is $\bar T = z$, $\bar C_j = C_j^{bot} + z$ for $j = 1, 2$ and $\bar\phi = \phi_0$ (constant solid fraction). In order to explicitly maintain the symmetry between components 1 and 2 and to exploit this symmetry in our interpretation of the results we reintroduce here the $\hat C_2$ variable. The disturbance equations are then

$$D^2\hat T - a^2\hat T - \hat w = \sigma\hat T, \tag{4.1a}$$

$$\frac{1 - \phi_0}{Le_j}(D^2\hat C_j - a^2\hat C_j) - \hat w - \frac{1}{Le_j}D\hat\phi = \sigma(1 - \phi_0)\hat C_j, \quad \text{for } j = 1, 2, \tag{4.1b}$$

$$\hat T - m_1\hat C_1 - m_2\hat C_2 = 0, \tag{4.1c}$$

$$D^2\hat w - a^2\hat w + a^2[Ra\hat T + Ra_1\hat C_1 + Ra_2\hat C_2] = 0, \tag{4.1d}$$

subject to $\hat T = \hat C_j = \hat w = 0$ at $z = 0, 1$ and $\hat\phi = 0$ at $z = 1$. While these equations omit a number of interactions associated with solidification – notably the effects of latent heat and solute rejection – the result is a set of disturbance equations whose linear

stability can be assessed analytically and interpreted more clearly. Note that the only remaining influence of solid fraction perturbations is through solute diffusion.

The disturbance equations given above differ in a number of ways from the classical ones describing double-diffusive convection in a non-reactive porous layer (e.g. Nield 1968; Nield & Bejan 1998). In this system there are two solute equations coupled by the solid fraction perturbation; this is a reactive porous layer in which phase transformation influences the overall solute balance. Here this influence occurs only through solute diffusion; in our more general model other effects such as solute rejection and latent heat release also play a role. Further, in the mushy layer context the solute fields are coupled with the thermal field directly through the liquidus constraint (4.1c). Alternatively, if we omit completely the variable $\hat{C}_2$ and its equation in (4.1b) and drop the $D\hat{\phi}$ term in the $\hat{C}_1$ equation and omit the liquidus constraint (4.1c) these equations reduce exactly to the classical double-diffusive ones. In the classical non-reactive porous case, while both real modes and oscillatory modes exist, only real modes are possible in a region of static stability. Further, for these instabilities occurring under statically stable conditions the system must be unstable with respect to the slower diffusing field. We shall see shortly in the present ternary mushy layer model that static instability with respect to an individual component (T, C_1 or C_2) is, remarkably, not a requirement for instability.

Solutions for the system of disturbance equations given in (4.1) take the form $\hat{T} = T^* \sin(n\pi z)$, $\hat{C}_j = C_j^* \sin(n\pi z)$, $\hat{w} = w^* \sin(n\pi z)$ and $\hat{\phi} = \phi^*[(-1)^n - \cos(n\pi z)]/(n\pi)$. The resulting characteristic equation is

$$0 = (1 - \phi_0) [J + \sigma(m_2 Le_1 + m_1 Le_2)] [J(J + \sigma) + a^2 Ra]$$
$$+ a^2 Ra_1 [m_2(Le_1 - Le_2)(J + \sigma) + (1 - \phi_0)(J + \sigma Le_2)]$$
$$+ a^2 Ra_2 [m_1(Le_2 - Le_1)(J + \sigma) + (1 - \phi_0)(J + \sigma Le_1)], \tag{4.2}$$

where $J = n^2\pi^2 + a^2$. The corresponding eigenfunction coefficients are given in the Appendix. With $\sigma = 0 + i\omega$ the real and imaginary parts of the characteristic equation are

$$0 = J^2 - \omega^2(m_2 Le_1 + m_1 Le_2) + a^2 Ra + a^2 Ra_1 \left[1 + \frac{m_2}{1 - \phi_0}(Le_1 - Le_2)\right]$$
$$+ a^2 Ra_2 \left[1 + \frac{m_1}{1 - \phi_0}(Le_2 - Le_1)\right], \tag{4.3a}$$

$$0 = \omega \left\{ J^2(1 + m_2 Le_1 + m_1 Le_2) + a^2 Ra(m_2 Le_1 + m_1 Le_2) + a^2 Ra_1 \right.$$
$$\left. \times \left[Le_2 + \frac{m_2}{1 - \phi_0}(Le_1 - Le_2)\right] + a^2 Ra_2 \left[Le_1 + \frac{m_1}{1 - \phi_0}(Le_2 - Le_1)\right] \right\}. \tag{4.3b}$$

Therefore, neutrally stable real modes ($\omega = 0$) satisfy

$$Ra + Ra_1 + Ra_2 + \frac{Le_1 - Le_2}{1 - \phi_0}(m_2 Ra_1 - m_1 Ra_2) = -\frac{J^2}{a^2}. \tag{4.4}$$

Also, neutrally stable oscillatory modes satisfy

$$Ra + Ra_1 + Ra_2 + \frac{\phi_0(Le_1 - Le_2)(m_2 Ra_1 - m_1 Ra_2)}{(1 - \phi_0)(m_2 Le_1 + m_1 Le_2)} = -\frac{J^2}{a^2}\left(1 + \frac{1}{m_2 Le_1 + m_1 Le_2}\right), \tag{4.5}$$

as long as $\omega^2 > 0$, where

$$\omega^2 = \frac{a^2}{m_2 Le_1 + m_1 Le_2} \left[\frac{J^2}{a^2} + Ra + Ra_1 + Ra_2 + \frac{Le_1 - Le_2}{1 - \phi_0}(m_2 Ra_1 - m_1 Ra_2) \right]. \quad (4.6)$$

For the case under consideration, the base-state temperature and composition profiles have $D\bar{T} = D\bar{C}_j = 1$ for $j = 1, 2$. Therefore, the condition representing static stability is

$$Ra + Ra_1 + Ra_2 = Ra_T + Ra_C > 0. \quad (4.7)$$

Consequently, (4.4) shows that except when $Le_1 = Le_2$ it is possible for neutrally stable real modes to exist in the statically stable region. That is to say (4.4) shows that neutrally stable real modes with $Ra + Ra_1 + Ra_2 > 0$ can exist with a sufficiently negative value of $(Le_1 - Le_2)(m_2 Ra_1 - m_1 Ra_2)$. Such modes could include cases in which up to two of the Rayleigh numbers are negative and would be suggestive of classical double-diffusive convection in which, taken individually, some fields are stabilizing and others are destabilizing. Even more interesting, however, is the fact that neutrally stable real modes can exist with each Rayleigh number individually positive. To demonstrate this possibility, consider the case $Le_1 > Le_2$ and fix positive values of Ra and Ra_1. Then, for a neutrally stable real mode a positive value Ra_2 is given by

$$Ra_2 = \frac{\dfrac{J^2}{a^2} + Ra + Ra_1 + \dfrac{m_2}{1 - \phi_0}(Le_1 - Le_2)Ra_1}{\dfrac{m_1}{1 - \phi_0}(Le_1 - Le_2) - 1}, \quad (4.8)$$

as long as Le_1 is sufficiently large (i.e. $Le_1 > Le_2 + (1 - \phi_0)/m_1$). A similar argument can be made if $Le_1 < Le_2$. Recall that a positive Ra along with $D\bar{T} = 1$ represents a stably stratified thermal field (and similarly for Ra_j and $D\bar{C}_j$), and so modes of instability with Ra, Ra_1 and Ra_2 all positive could not be characterized as standard buoyant modes of instability. Further, they are also different from classical double-diffusive modes that occur in statically stable regions; such modes require instability with respect to one of the two diffusing components. Our results here indicate the presence of a novel mode of convective instability that can exist even when the system is stably stratified with respect to all thermal and solutal fields individually.

A simple example that highlights the interactions and essential mechanism of this instability is the case with $Ra = Ra_1 = 0$. Here T and C_1 make no contribution to buoyancy. Further, since $D\bar{C}_2 = 1$ the system is arguably stably stratified with respect to C_2 when $Ra_2 > 0$. Equation (4.4) shows that a real mode of instability exists when

$$Ra_2 \left[1 + m_1 \frac{Le_2 - Le_1}{1 - \phi_0} \right] = -\frac{J^2}{a^2}. \quad (4.9)$$

When $Le_1 = Le_2$ a standard buoyant mode of instability (with $Ra_2 < 0$) is predicted. However, when Le_1 is sufficiently large (specifically, $Le_1 > Le_2 + (1 - \phi_0)/m_1$) the neutrally stable modes have $Ra_2 > 0$. Thus, despite an apparently statically stable C_2 profile (and no buoyant effects associated with T or C_1) an instability occurs.

The above-given example suggests the following parcel argument, which for physical interpretation we give in terms of original unscaled temperature and composition variables. Consider a setting in which a layer of fluid is cool and rich with respect to both solute fields at the bottom and warm and fresh with respect to both solute fields at the top. For simplicity we shall assume that there are no buoyant effects associated with the temperature field or composition 1 (i.e. $\alpha = \alpha_1 = 0$ or $Ra = Ra_1 = 0$) and that fluid rich in composition 2 is denser (i.e. $\alpha_2 < 0$ in (2.7) which also corresponds to $Ra_2 > 0$, since $\Delta C_2' < 0$ in this case). Arguably this is a stably stratified layer from a static point of view. Further, suppose that $Le_1 \gg Le_2 \gg 1$ so that composition 1 is the slowest diffusing field and the temperature is the fastest diffusing field. Now we displace a parcel of fluid upwards. This fluid parcel rapidly equilibrates to its new (warmer) thermal environment. In contrast the solute field C_1' diffuses extremely slowly and hence remains richer than its environment. The solute field C_2' meanwhile is forced to maintain thermodynamic equilibrium (via the liquidus constraint) and with the help of changes in solid fraction via freezing or dissolution must overcompensate for the sluggishness of the C_1' field in order to keep up with the efficiently diffusing thermal field. The net effect is for the parcel to become correspondingly fresher in C_2' than its local environment. This reduced value of C_2' makes the parcel lighter than its surroundings (recall that only C_2' contributes to buoyancy in this simple example) and provides an upward buoyant force, thus generating a direct mode of instability. This argument suggests that the instability is a manifestation of an interplay between the rapidly diffusing thermal field, the slowest diffusing solute field and the buoyant response of the other solute field as well as the constraint of thermodynamic equilibrium. A similar argument would apply if $Le_2 \gg Le_1$; here a positive value of Ra_1 would be required (see also (4.8)).

Figure 7 gives a visual description of the new instability and the corresponding parcel argument. On the left are shown sketches of five typical base-state solidification paths (heavy solid lines) similar to the five base-state solutions in figure 2. The layer is colder and richer in the two compositions at the bottom. The heavy dashed lines show lines of constant density chosen here to represent the case with $Ra = Ra_1 = 0$ and $Ra_2 > 0$. The heavy dash-dotted lines show representative isotherms (corner 3 is the warmest). Lines parallel to the 1–3 side of the diagram correspond to lines of constant C_2'. Similarly, lines parallel to the 2–3 side correspond to lines of constant C_1'. Here only base state 1 has a non-monotonic density profile; there is a region of heavy fluid between regions of light fluid above and below. The four other base-state solutions shown are stable from a static point of view; the density decreases from bottom to top. Note that changing the three Rayleigh numbers has the effect of rotating the lines of constant density relative to the solidification paths shown, and so, with the exception of base state 3, any base-state solution can have a non-monotonic density profile depending on the Rayleigh numbers. The diagram on the right presents another view of the parcel argument given above for the real mode of instability and demonstrates how a statically stable base-state solution can be linearly unstable to perturbations. Consider a parcel initially at point P that is displaced from its original isotherm to a new isotherm associated with points Q and R. The parcel quickly adjusts to the new local temperature, but owing to the slow diffusing C_1' field, it remains (at least approximately) on a horizontal line corresponding to fixed C_1'. In order to maintain this C_1' and remain on the isotherm, the parcel adjusts its C_2' value, and its new composition corresponds to point R. However, fluid with composition R is less dense than the surrounding fluid, whose base-state
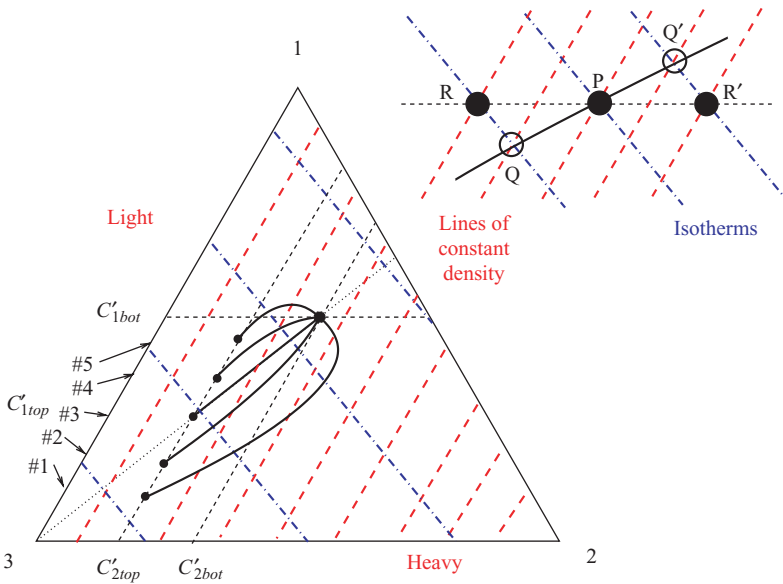
FIGURE 7. The figure shows a sketch of five typical solidification paths in the composition plane of the ternary phase diagram. The heavy dashed lines indicate lines of constant density chosen here for simplicity to correspond to lines of constant C_2. The heavy dash-dotted lines correspond to isotherms. The diagram on the right shows that when a parcel initially at point P is displaced to a new isotherm (containing points Q and R) a slowly diffusing C_1 field forces the parcel to maintain composition of point R whose density is less than its local density of point Q. When the density trend is reversed (exchange 'heavy' with 'light') a fluid parcel can oscillate between point R at which the parcel is relatively heavy and point R' at which the parcel is relatively light.

composition and density correspond to point Q, and hence a direct mode of instability occurs.

The instability observed here shares some of its unusual traits with the so-called anti-convection first identified theoretically by Welander (1964). In the work of Welander (1964) and more recent work by Gershuni & Zhukhovitskii (1980) and Perestenko & Ingel (1995) a convective instability is predicted in a system of two horizontal fluid layers heated from above, which from a static point of view would appear to be stably stratified. Surface tension or Marangoni-driven flows were not included in these models, although the later work of Perestenko & Ingel (1995) did introduce effects of evaporation. This 'anti-convection' is predicted to occur when the fluid in the upper layer has small thermal diffusivity and thermal expansion coefficient relative to those of the fluid in the lower layer. For this situation, when a fluid parcel in the upper layer near the interface is displaced downwards, its temperature is slow to respond owing to the small thermal diffusivity, and it experiences little restoring force owing to the weak buoyant response of the upper layer. At the same time, a local region of fluid in the lower layer warms relatively quickly in response to the above nearby warm parcel. This generates a density differential in the lower layer that owing to the strong buoyant response of the lower layer drives convection outwards along the interface. The upper fluid responds to the resultant shear force and generates convection in the upper layer that enhances the motion of the displaced parcel, driving the instability. Thus, despite an overall stabilizing thermal gradient a convective instability related to a non-trivial interaction between diffusion and buoyancy is predicted.

We return to the oscillatory mode in our simplified ternary model and note that by using (4.5) two additional forms for ω^2 given in (4.6) are

$$\omega^2 = -\frac{a^2}{m_2 Le_1 + m_1 Le_2}\left[\frac{J^2}{a^2}\left(\frac{m_2 Le_1 + m_1 Le_2 + 1 - \phi_0}{\phi_0}\right)\right.$$

$$\left. + (Ra + Ra_1 + Ra_2)\left(\frac{m_2 Le_1 + m_1 Le_2}{\phi_0} - 1\right)\right] = \frac{a^2}{(m_2 Le_1 + m_1 Le_2)^2}$$

$$\times \left[-\frac{J^2}{a^2} + \frac{(m_2 Le_1 + m_1 Le_2 - \phi_0)(Le_1 - Le_2)(m_2 Ra_1 - m_1 Ra_2)}{1 - \phi_0}\right]. \quad (4.10)$$

The first form for ω^2 shows that under typical conditions with $m_2 Le_1 + m_1 Le_2 > \phi_0$, it is not possible to have an oscillatory mode (i.e. $\omega^2 > 0$) unless $Ra + Ra_1 + Ra_2$ is sufficiently negative; no oscillatory mode is expected in the statically stable region $Ra + Ra_1 + Ra_2 > 0$. The second form for ω^2 shows that the oscillatory mode cannot exist unless $(Le_1 - Le_2)(m_2 Ra_1 - m_1 Ra_2)$ is sufficiently positive. For example, if $Le_1 > Le_2$, then for an oscillatory mode to exist $m_2 Ra_1 - m_1 Ra_2 = m_2 Ra_C$ must be positive. Furthermore, since $Ra + Ra_1 + Ra_2 = Ra_T + Ra_C$ is required to be sufficiently negative, Ra_T must be negative. One possible combination of Ra, Ra_1 and Ra_2 that gives rise to the case $Ra_T < 0$ and $Ra_C > 0$ is with $Ra_2 = 0$, $Ra < 0$ and $Ra_1 > 0$. This is similar to the standard double-diffusive oscillatory mode in a non-reactive porous layer where the faster diffusing thermal field is destabilizing and the slower diffusing solute field is stabilizing. However, other combinations of Ra, Ra_1 and Ra_2 give rise to an oscillatory mode and as described below can be interpreted through a different mechanism.

Consider again the case with no buoyancy associated with T and C_1 (i.e. $Ra = Ra_1 = 0$) and $Le_1 \gg Le_2$. Here an oscillatory mode is possible for a sufficiently negative value of Ra_2. In the diagram given in figure 7 with warmer and fresher fluid above colder and richer fluid, negative Ra_2 (along with $Ra = Ra_1 = 0$) is consistent with exchanging the labels 'heavy' and 'light'. Then, a parcel displaced from point P to the isotherm associated with points Q and R will again take on the composition of point R by the same argument given earlier for the real mode. Now the parcel at R is heavier than that of its surrounding fluid at composition Q. This creates an oscillatory motion in which the fluid parcel has additional gravitational mass at the top of its cycle (point R), is forced back down past its original position to the bottom of its cycle (point R′) where it is correspondingly lighter than the surrounding fluid at composition Q′ and is consequently forced back up. This oscillatory mode is novel in the sense that there is no statically stable thermal or solute field present to support an oscillation. Rather, the constraint of thermodynamic equilibrium in the mushy layer along with a slowly diffusing C_1 field and a rapidly diffusing thermal field both supports the oscillations and allows them to grow.

Owing to the liquidus constraint, the three Rayleigh numbers Ra, Ra_1 and Ra_2 influence the stability of the system only through the two effective Rayleigh numbers Ra_T and Ra_C. This highlights a degeneracy in which more than one combination of Ra, Ra_1 and Ra_2 gives rise to a single coordinate point (Ra_T, Ra_C). With this in mind, we show graphically a set of stability boundaries in the Ra_C-versus-Ra_T plane in figure 8 representing the most dangerous neutral modes ($n = 1$) given by (4.4) and (4.5). We identify several notable regions in these plots. First, the boundaries
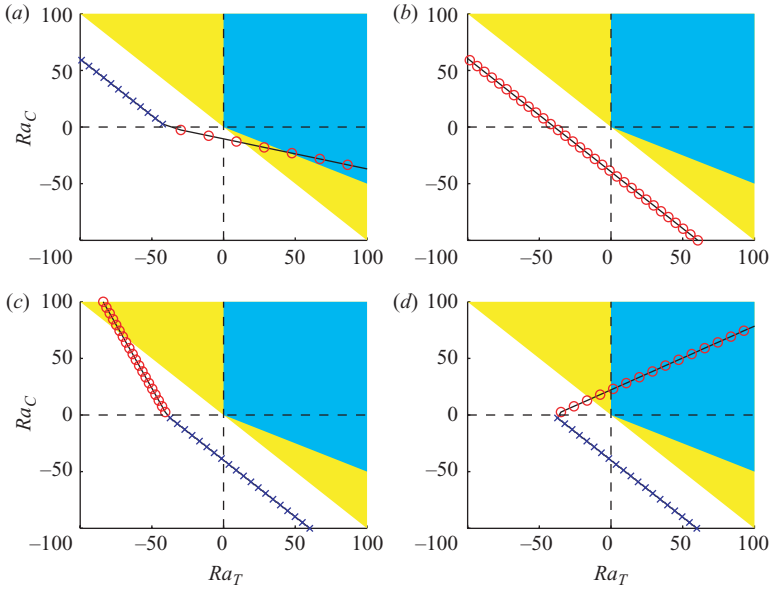
FIGURE 8. The figure shows four stability plots indicating the most dangerous neutral modes ($n = 1$) from (4.4) and (4.5) for $Le_2 = 100$, $m_1 = m_2 = 0.5$ and $\phi_0 = 0.1$ and (a) $Le_1 = 105$, (b) $Le_1 = 100$, (c) $Le_1 = 99$ and (d) $Le_1 = 95$.

marked with 'o' indicate real modes, while the boundaries marked with '×' indicate oscillatory modes and separate stable regions (on the right) from unstable regions (on the left). These boundaries correspond to critical points, which in this simplified model always occur at wavenumber $a = \pi$, along neutral stability curves in the Rayleigh-number-versus-wavenumber space. Second, the shaded regions (either yellow or cyan) indicate as before where the base-state solution is statically stable; that is to say the base state has $G_\rho < 0$ when $Ra_T + Ra_C = Ra + Ra_1 + Ra_2 > 0$. Additionally, following from (2.12), the cyan-shaded region, defined by $Ra_T > 0$ and $Ra_C > -m_1 Ra_T$, indicates where it is possible for Ra, Ra_1 and Ra_2 to be simultaneously positive. For example, in figure 8(d) one could identify an unstable mode corresponding to positive values of Ra, Ra_1 and Ra_2 at the point $Ra_T = 25$, $Ra_C = 50$ (namely $Ra_1 = (m_1/m_2)Ra_2 + 50$ and $Ra = 25 - Ra_2/m_2$ for a sufficiently small but positive Ra_2 value). Similar regions are shown in figure 8(a). This once again displays the surprising result that scenarios exist for which a real mode of instability is present despite the fact that all thermal and solute fields are individually stabilizing. It is of course also possible for combinations with Ra, Ra_1 and Ra_2 not all positive to correspond to points in these shaded regions. These plots also show that an oscillatory mode is always present when $Le_1 \neq Le_2$ but never occurs in the statically stable region. The results of the previous section show that while oscillatory modes can exist for more general cases with $Le_1 = Le_2$ they still do not occur in the statically stable region.

We briefly return to (4.1) to make a final observation associated with the above-mentioned instabilities. If one eliminates the variable $\hat{C}_2$ in (4.1) using the liquidus constraint, a reduced system becomes

$$D^2 \hat{T} - a^2 \hat{T} - \hat{w} = \sigma \hat{T}, \qquad (4.11a)$$

$$\frac{1-\phi_0}{Le_1}(D^2\hat{C}_1 - a^2\hat{C}_1) - \hat{w} - \frac{1}{Le_1}D\hat{\phi} = \sigma(1-\phi_0)\hat{C}_1, \qquad (4.11b)$$

$$D\hat{\phi} + [m_1 Le_1 + m_2 Le_2 - (1-\phi_0)]\,\hat{w} = -\sigma(1-\phi_0)\left[m_1(Le_1 - Le_2)\hat{C}_1 + (Le_2 - 1)\hat{T}\right], \qquad (4.11c)$$

$$D^2\hat{w} - a^2\hat{w} + a^2[Ra_T\hat{T} + Ra_C\hat{C}_1] = 0. \qquad (4.11d)$$

Further noting that the term $D\hat{\phi}$ can be eliminated from these equations leads to a set of equations for $\hat{T}$, $\hat{C}_1$ and $\hat{w}$ given by (4.11a), (4.11d) and

$$\frac{1-\phi_0}{Le_1}\left(D^2\hat{C}_1 - a^2\hat{C}_1\right) - \left\{\frac{m_2(Le_1 - Le_2) + 1 - \phi_0}{Le_1}\right\}\hat{w} = \sigma(1-\phi_0)$$
$$\times \left\{\frac{m_2 Le_1 + m_1 Le_2}{Le_1}\hat{C}_1 - \frac{Le_2 - 1}{Le_1}\hat{T}\right\}. \quad (4.12)$$

In contrast with the classical problem of double-diffusive convection in a non-reactive porous layer in which a linear composition profile leads to a constant coefficient on the advective term, the $\hat{C}_1$ equation (4.12) has a $\hat{w}$ coefficient whose sign depends on the relative size of Le_1 and Le_2 as well as m_2 and ϕ_0. The broken symmetry between indices 1 and 2 here reflects the asymmetry with respect to these indices in the effective Rayleigh numbers as well as the elimination of $\hat{C}_2$ from the equations. A change in sign of this coefficient has a dynamic effect similar to a change in the sign of the base-state gradient $d\bar{C}_1/dz$. For a neutrally stable real mode with $\sigma = 0$ one can deduce from these equations that a sign change of the $\hat{w}$ term in (4.12) leads to a sign change in $\hat{C}_1$, which from (4.11d) leads to a sign change in Ra_C.

5. Conclusions

We have investigated convective instabilities in a ternary alloy mushy layer model that includes diffusion of heat and solute as well as thermodynamic equilibrium constraints associated with mushy layer solidification. Our results reveal that double-diffusive-type convection can occur in these systems. Additionally, new novel modes of instability – both real and oscillatory – are predicted. These modes have been identified analytically as well as numerically and appear to be robust features of our model.

Parcel arguments for these real and oscillatory modes suggest that they both result from interactions between the coupling of the fluid with solidification processes within the mushy layer (linking the thermal and solute fields through the thermodynamic equilibrium constraint) and the independent nature of the fluid temperature and composition as dictated by the disparate rates at which diffusion of these fields occur. The solidification and diffusion processes can thus be at odds with each other and conspire to generate instabilities under unexpected conditions. A real mode of instability, driven by these interactions, is predicted even in the absence of static instability with respect to any of the individual thermal or compositional profiles. Alternately, an oscillatory instability can be identified under conditions in which there are no other statically stable solute or thermal gradients to support it.

Work attempting to further quantify these instabilities in full multi-layer ternary systems is currently underway. We hope that our results will inspire investigation to see how and if these instabilities manifest themselves in laboratory settings. More

generally, we hope that the novel interactions identified here will lead to further understanding of convective phenomena in fluid–solidification coupled systems.

Appendix. Eigenfunction coefficients

The eigenfunction coefficients in the simplified ternary alloy model are $T^* = 1$ and

$$w^* = -(\sigma + J), \tag{A 1a}$$

$$C_1^* = \frac{m_2(Le_1 - Le_2)(\sigma + J) + (1 - \phi_0)(\sigma Le_2 + J)}{(1 - \phi_0)[J + \sigma(m_2 Le_1 + m_1 Le_2)]}, \tag{A 1b}$$

$$C_2^* = \frac{m_1(Le_2 - Le_1)(\sigma + J) + (1 - \phi_0)(\sigma Le_1 + J)}{(1 - \phi_0)[J + \sigma(m_2 Le_1 + m_1 Le_2)]}, \tag{A 1c}$$

$$\phi^* = (m_1 Le_1 + m_2 Le_2)(\sigma + J) - (1 - \phi_0)J$$
$$- \sigma m_1 Le_1 \left[\frac{m_2(Le_1 - Le_2)(\sigma + J) + (1 - \phi_0)(\sigma Le_2 + J)}{J + \sigma(m_2 Le_1 + m_1 Le_2)} \right]$$
$$- \sigma m_2 Le_2 \left[\frac{m_1(Le_2 - Le_1)(\sigma + J) + (1 - \phi_0)(\sigma Le_1 + J)}{J + \sigma(m_2 Le_1 + m_1 Le_2)} \right]. \tag{A 1d}$$

REFERENCES

AITTA, A., HUPPERT, H. E. & WORSTER, M. G. 2001a Diffusion-controlled solidification of a ternary melt from a cooled boundary. *J. Fluid Mech.* **432**, 201–217.

AITTA, A., HUPPERT, H. E. & WORSTER, M. G. 2001b Solidification in ternary systems. In *Interactive Dynamics of Convection and Solidification* (ed. P. Ehrhard, D. S. Riley & P. H. Steen), pp. 113–122. Kluwer.

AMBERG, G. & HOMSY, G. M. 1993 Nonlinear analysis of buoyant convection in binary solidification with application to channel formation. *J. Fluid Mech.* **252**, 79–98.

ANDERSON, D. M. 2003 A model for diffusion-controlled solidification of ternary alloys in mushy layers. *J. Fluid Mech.* **483**, 165–197.

ANDERSON, D. M. & SCHULZE, T. P. 2005 Linear and nonlinear convection in solidifying ternary alloys. *J. Fluid Mech.* **545**, 213–243.

ANDERSON, D. M. & WORSTER, M. G. 1995 Weakly-nonlinear analysis of convection in a mushy layer during the solidification of binary alloys. *J. Fluid Mech.* **302**, 307–331.

ANDERSON, D. M. & WORSTER, M. G. 1996 A new oscillatory instability in a mushy layer during the solidification of binary alloys. *J. Fluid Mech.* **307**, 245–267.

BLOOMFIELD, L. J. & HUPPERT, H. E. 2003 Solidification and convection of a ternary solution cooled from the side. *J. Fluid Mech.* **489**, 269–299.

BOETTINGER, W. J., KATTNER, U. R., CORIELL, S. R., CHANG, Y. A. & MUELLER, B. A. 1995 Development of multicomponent solidification micromodels using a thermodynamic phase diagram data base. In *Modelling of Casting, Welding and Advanced Solidification Processes VII* (ed. M. Cross & J. Campbell), pp. 649–656. TMS.

CANUTO, C., HUSSAINI, M. Y., QUARTERONI, A. & ZANG, T. A. 1988 *Spectral Methods in Fluid Dynamics.* Springer.

CHEN, F., LU, J. W. & YANG, T. L. 1994 Convective instability in ammonium chloride solution directionally solidified from below. *J. Fluid Mech.* **276**, 163–187.

CHUNG, C. A. & CHEN, F. 2000 Onset of plume convection in mushy layers. *J. Fluid Mech.* **408**, 53–82.

CHUNG, C. A. & WORSTER, M. G. 2002 Steady-state chimneys in a mushy layer. *J. Fluid Mech.* **455**, 387–411.

CORIELL, S. R., CORDES, M. R., BOETTINGER, W. J. & SEKERKA, R. F. 1980 Convective and interfacial instabilities during unidirectional solidification of a binary alloy. *J. Cryst. Growth* **49**, 13–28.

DAVIS, S. H. 2001 *Theory of Solidification*. Cambridge University Press.

FELICELLI, S. D., POIRIER, D. R. & HEINRICH, J. C. 1997 Macrosegregation patterns in multicomponent Ni-base alloys. *J. Cryst. Growth* **177**, 145–161.

FELICELLI, S. D., POIRIER, D. R. & HEINRICH, J. C. 1998 Modeling freckle formation in three dimensions during solidification of multicomponent alloys. *Metall. Mat. Trans.* B **29**, 847–855.

FLYNN, T. J. 2009 Linear Stability Analysis of a Solidifying Ternary Alloy. Master's thesis, George Mason University, Fairfax, VA.

GERSHUNI, G. Z. & ZHUKOVITSKII, E. M. 1980 Instability of a system of horizontal layers of immiscible fluids heated from above. *Fluid Dyn.* **15**, 816–822. Originally published in Russian in *Izv. Akad. Nauk SSSR, Mekh. Zhidk. Gaza* **6**, 28–34.

GRIFFITHS, R. W. 1979 The influence of a third diffusing component upon the onset of convection. *J. Fluid Mech.* **92**, 659–670.

GUBA, P. & WORSTER, M. G. 2006a Nonlinear oscillatory convection in mushy layers. *J. Fluid Mech.* **553**, 419–443.

GUBA, P. & WORSTER, M. G. 2006b Free convection in laterally solidifying mushy regions. *J. Fluid Mech.* **558**, 69–78.

HUPPERT, H. E. & SPARKS, R. S. J. 1984 Double-diffusive convection due to crystallization in magmas. *Annu. Rev. Earth Planet. Sci.* **12**, 11–37.

HUPPERT, H. E. & TURNER, J. S. 1981 Double-diffusive convection. *J. Fluid Mech.* **106**, 299–329.

HURLE, D. T. J., JAKEMAN, E. & WHEELER, A. A. 1982 Effect of solutal convection on the morphological stability of a binary alloy. *J. Cryst. Growth* **58**, 163–179.

KATZ, R. F. & WORSTER, M. G. 2008 Simulation of directional solidification, thermochemical convection, and chimney formation in a Hele–Shaw cell. *J. Comput. Phys.* **227**, 9823–9840.

KELLER, H. B. 1976 *Numerical Solution of Two Point Boundary Value Problems*, Regional Conference Series in Applied Mathematics, vol. 24. SIAM.

KRANE, M. J. M. & INCROPERA, F. P. 1997 Solidification of ternary metal alloys–II. Prediction of convective phenomena and solidification behaviour of Pb–Sb–Sn alloys. *Intl J. Heat Mass Transfer* **40**, 3837–3847.

KRANE, M. J. M., INCROPERA, F. P. & GASKELL, D. R. 1998 Solidification of a ternary metal alloy: a comparison of experimental measurements and model predictions in a Pb–Sb–Sn system. *Metall. Mat. Trans.* A **29**, 843–853.

LAN, C. W. & TU, C. Y. 2000 Morphological instability due to double diffusive convection in directional solidification: the pit formation. *J. Cryst. Growth* **220**, 619–630.

LUPIS, C. H. P. 1993 *Chemical Thermodynamics of Materials*. MIT.

NANDAPURKAR, P., POIRIER, D. R., HEINRICH, J. C. & FELICELLI, S. 1989 Thermosolutal convection during dendritic solidification of alloys. Part I. Linear stability analysis. *Metall. Trans.* B **20**, 711–721.

NIELD, D. A. 1968 Onset of thermohaline convection in a porous medium. *Water Resour. Res.* **4**, 553–560.

NIELD, D. A. & BEJAN, A. 1998 *Convection in Porous Media*. Springer.

PERESTENKO, O. V. & INGEL, L. KH. 1995 The occurrence of moist 'anticonvection' in a water–air system. *J. Fluid Mech.* **287**, 1–20.

POULIKAKOS, D. 1985 The effect of a third diffusing component on the onset of convection in a horizontal porous layer. *Phys. Fluids* **28**, 3172–3174.

ROPER, S. M., DAVIS, S. H. & VOORHEES, P. W. 2007 Convection in a mushy zone forced by sidewall heat losses. *Metall. Mat. Trans.* A **38A**, 1069–1079.

ROPER, S. M., DAVIS, S. H. & VOORHEES, P. W. 2008 An analysis of convection in a mushy layer with a deformable permeable interface. *J. Fluid Mech.* **596**, 333–352.

RUDRAIAH, N. & VORTMEYER, D. 1982 The influence of permeability and of a third diffusing component upon the onset of convection in a porous medium. *Intl J. Heat Mass Trans.* **25**, 457–464.

SCHAEFFER, R. J. & CORIELL, S. R. 1984 Convection-induced distortion of a solid–liquid interface. *Metall. Trans.* A **15**, 2109–2115.

SCHNEIDER, M. C., GU, J. P., BECKERMANN, C., BOETTINGER, W. J. & KATTNER, U. R. 1997 Modeling of micro- and macrosegregation and freckle formation in single-crystal nickel-base superalloy directional solidification. *Metall. Mat. Trans.* A **28**, 1517–1531.

SCHULZE, T. P. & WORSTER, M. G. 1998 A numerical investigation of steady convection in mushy layers during the directional solidification of binary alloys. *J. Fluid Mech.* **356**, 199–220.

SCHULZE, T. P. & WORSTER, M. G. 1999 Weak convection, liquid inclusions and the formation of chimneys in mushy layers. *J. Fluid Mech.* **388**, 197–215.

SCHULZE, T. P. & WORSTER, M. G. 2001 Mushy zones with fully developed chimneys. In *Interactive Dynamics of Convection and Solidification* (ed. P. Ehrhard, D. S. Riley & P. H. Steen), pp. 71–80. Kluwer.

SCOTT, M. R. & WATTS, H. A. 1977 Computational solution of linear two-point boundary value problems via orthonormalization. *SIAM J. Numer. Anal.* **14**, 40–70.

SINGH, A. K. & BASU, B. 1995 Mathematical modelling of macrosegregation of iron carbon binary alloy: role of double diffusive convection. *Metall. Mater. Trans.* B **26**, 1069–1081.

SMALLMAN, R. E. & BISHOP, R. J. 1999 *Modern Physical Metallurgy and Materials Engineering*. Butterworth-Heinemann.

THI, H. N., BILLIA, B. & JAMGOTCHIAN, H. 1989 Influence of thermosolutal convection on the solidification front during upwards solidification. *J. Fluid Mech.* **204**, 581–597.

THOMPSON, A. F., HUPPERT, H. E. & WORSTER, M. G. 2003*a* A global conservation model for diffusion-controlled solidification of a ternary alloy. *J. Fluid Mech.* **483**, 191–197.

THOMPSON, A. F., HUPPERT, H. E., WORSTER, M. G. & AITTA, A. 2003*b* Solidification and compositional convection of a ternary alloy. *J. Fluid Mech.* **497**, 167–199.

TREFETHEN, L. N. 2000 *Spectral Methods in Matlab*. SIAM.

TURNER, J. S. 1973 *Buoyancy Effects in Fluids*. Cambridge University Press.

WELANDER, P. 1964 Convective instability in a two-layer fluid heated uniformly from above. *Tellus* **16**, 349–358.

WORSTER, M. G. 1986 Solidification of an alloy from a cooled boundary. *J. Fluid Mech.* **167**, 481–501.

WORSTER, M. G. 1992*a* Instabilities of the liquid and mushy regions during solidification of alloys. *J. Fluid Mech.* **237**, 649–669.

WORSTER, M. G. 1992*b* The dynamics of mushy layers. In *Interactive Dynamics of Convection and Solidification* (ed. S. H. Davis, H. E. Huppert, U. Muller & M. G. Worster), pp. 113–138. Kluwer.

WORSTER, M. G. 1997 Convection in mushy layers. *Annu. Rev. Fluid Mech.* **29**, 91–122.

WORSTER, M. G. 2000 Solidification of fluids. In *Perspectives in Fluid Dynamics* (ed. G. K. Batchelor, H. K. Moffatt & M. G. Worster), pp. 393–446. Cambridge University Press.